

Molecular Dynamics Study of Li⁺ Migration through Graphene Membranes

A. E. Galashev^{a, z} and Yu. P. Zaikov^{a, b}

^a Institute of High Temperature Electrochemistry, Ural Branch, Russian Academy of Sciences, ul. S. Kovalevskoi 22, Yekaterinburg, 620137 Russia

^b Ural Federal University named after the first President of Russia B.N. Yeltsin, ul. Mira 19, Yekaterinburg, 620002 Russia

Received September 23, 2014

Abstract—The throughput of six combinations of modified graphene membranes as regards the penetration of lithium ions is studied by a molecular dynamics method. The membrane modification involves formation of four types of pores and their partial hydrogenation. The best throughput capacity is demonstrated by a pair of membranes with pores represented by bivacancies. In this case, the mobility of lithium ions is the highest in the vertical driving-force direction and the lowest in the horizontal directions. The average level to which the ions in the basic cell are elevated serves as a reliable criterion of efficiency of the device studied. The increase in membrane throughput is associated with weakening of local stresses created by both horizontal and vertical forces.

Keywords: graphene, defects, lithium ion, channel, molecular dynamics, stress, mobility

DOI: 10.1134/S1023193515090050

INTRODUCTION

Since its discovery, graphene or monolayer graphite attracts keen attention. Due to its two-dimensional structure, graphene has several unusual physical and chemical properties. For instance, at low energies, the electrons and holes can be described in good approximation by the Dirac equation [1], and this seems to be an excellent method for testing the quantum electro-dynamics phenomena.

Graphene can be synthesized from graphene oxide in large amounts and at low cost [2]. The advantage provided by the graphene low cost and high electric conductivity stimulates the development of graphene-based supercapacitors. However, despite all the efforts undertaken, it is still difficult to obtain supercapacitors with the high specific capacitance. The main explanation is that graphene sheets thus prepared tend to spontaneous aggregation. To a certain extent, this problem can be solved by using nanoporous graphene synthesized based on chemically activated graphene oxide microwave-split in the presence of KOH [3]. Such electrode material is characterized by the high values of conductivity and specific surface area ($\sim 3100 \text{ m}^2 \text{ g}^{-1}$). Its use in industry has good prospects.

Functionalized graphene sheets were used in lithium-air batteries to provide the high electrochemical capacity ($\sim 15000 \text{ mA h/g}$) [4]. However, because the preparation of graphene electrodes with 2D geometry is very difficult, these electrodes were made of hierarchi-

cal porous graphene with the 3D geometry. During the discharge, the strong large tunnels present in electrodes provided the fast access of oxygen from environmental air and the small pores in walls served as “ways out” for oxygen, thus maintaining the three-phase state (solid–liquid–gas). The deposits of reaction products (such as Li_2O_2) on the carbon electrode eventually blocked the oxygen access, limiting the capacity of the lithium-air battery. The open 2D structure of the electrode in this battery could be more efficient were the necessary gaps between graphene sheets sustained during the electrode charging–discharge processes.

In graphene, the Fermi level is localized between two symmetrical conic zones that contact the Fermi level in six spaced points called the Dirac points which are localized on the edges of the hexagonal Brillouin zone. In the vicinity of these points, the zero-excitation energy operates. Graphene has the linear energy spectrum of the Dirac type in the vicinity of each of 6 singular points. The linear dispersion near these points means that the charge carriers in graphene can be considered as zero-mass relativistic particles. This gives rise to many unusual phenomena such as the Hall quantum effect [1] or the Klein paradox [5]. However, the Dirac equation describes not the motion of an individual particle but the time evolution of the quantum field in which antiparticles are also present. According to calculations, the electron is completely reflected from a barrier and the electron–positron pairs are formed in the barrier [6]. In contrast to the case of zero-mass Dirac fermions for which the barrier

^z Corresponding author: galashev@iht.euran.ru (A.E. Galashev).

Table 1. Versions of membrane combinations in the basic cell (type and number of vacancies and the number of atoms C in the upper and lower membranes)

Membranes parameters	Versions					
	1	2	3	4	5	6
Type and number of pores in the lower membrane	Monovacancies 9	Bivacancies 9	Trivacancies 9	Bivacancies 9	Trivacancies 9	Hexavacancies 6
Type and number of pores in the upper membrane	Bivacancies 9	Trivacancies 9	Hexavacancies 6	Bivacancies 9	Trivacancies 9	Hexavacancies 6
Number of C atoms in the lower membrane	397	388	379	388	379	370
Number of C atoms in the upper membrane	388	379	370	388	379	370

is totally transparent in case of normal incidence, the probability of charge transfer from nonzero-mass carriers is below unity and depends on the Brillouin zone index [7]. The probability P of tunneling for normal incidence is approximately proportional to $\exp(-2kd)$ [8], where k is the wave vector (oriented in the direction perpendicular to the barrier) and d is the barrier width. The electron energy is proportional to k : $E_e = \hbar\omega = \hbar kc$, where c is the light velocity. Hence, the dependence $P(d, E_b)$ exponentially decreases with the potential-barrier width and height E_b . As applied to our model, the paradox lies in the fact that due to small d of graphene, for all really observed k values, the value of P is close to 1 for any ion in contact with graphene. However, the physical transfer of a charge carrier does not occur upon its collision with graphene and the carrier retains its electrical properties.

The present model reflects the diffusion of Li^+ ions in a planar anode of the lithium–air battery where oxygen supplied from air serves in fact as the cathode. The battery discharge produces Li_2O_2 . The percentage of oxygen ions in air is not very high. The oxidation reaction also does not produce free oxygen ions O^{-2} . Hence, the model assumes the absence of negative ions. The cathodic processes are beyond our consideration.

The interaction of carbon materials with hydrogen was considered earlier as applied to hydrogen storage in solids [9]. The encouraging results were produced by functionalizing graphite basal planes (graphene) with hydrogen atoms. Hydrogen was adsorbed uniformly throughout the whole graphene surface, which eventually produced a stable material [10]. At present, it is known that lithium clusters represent a wonderful material for hydrogen storage [11]. The nature of hydrogen interaction with lithium clusters was studied

both theoretically and experimentally; in particular, the possibility was demonstrated for hydrogenization of lithium clusters [12]. Molecular dynamics (MD) density-functional simulations [11] have shown that the hydrogen atom passes from the graphene layer to the lithium cluster at 300 K and atmospheric pressure with the binding energy exceeding the corresponding energy of the hydrogen atom in the graphene layer.

The purpose of the present study was to consider the possibility of charging a planar graphene electrode in the lithium–air battery representing two functionalized graphene sheets with six different versions of pores.

COMPUTER MODEL

The basic cell of the model represents a rectangular parallelepiped elongated along the oz axis with the planes impermeable for Li^+ ions. The boundary conditions operating on the planes correspond to the reflection of totally elastic balls from a wall. In its middle part, the parallelepiped is divided into parts by two parallel membranes of defective graphene. The size of graphene sheets was 3.2×2.8 nm. Each membrane contained 6 or 9 pores of certain size which were distributed approximately uniformly over the graphene sheet. Figure 1 shows the types of membranes used. The pores in the upper membrane were shifted by a value not exceeding the graphene lattice period in order to prevent the direct vertical crossing of two membranes at once by a Li^+ ion. The upper and the lower membranes could be of either identical or different types. Table 1 shows numbers of basic cells with different types of membranes. Thus, each of 6 basic cells was divided into three chambers, i.e., lower, middle (between two graphene membranes), and upper chambers with the equal height of 0.6 nm. An additional calculation has shown that this very gap provides

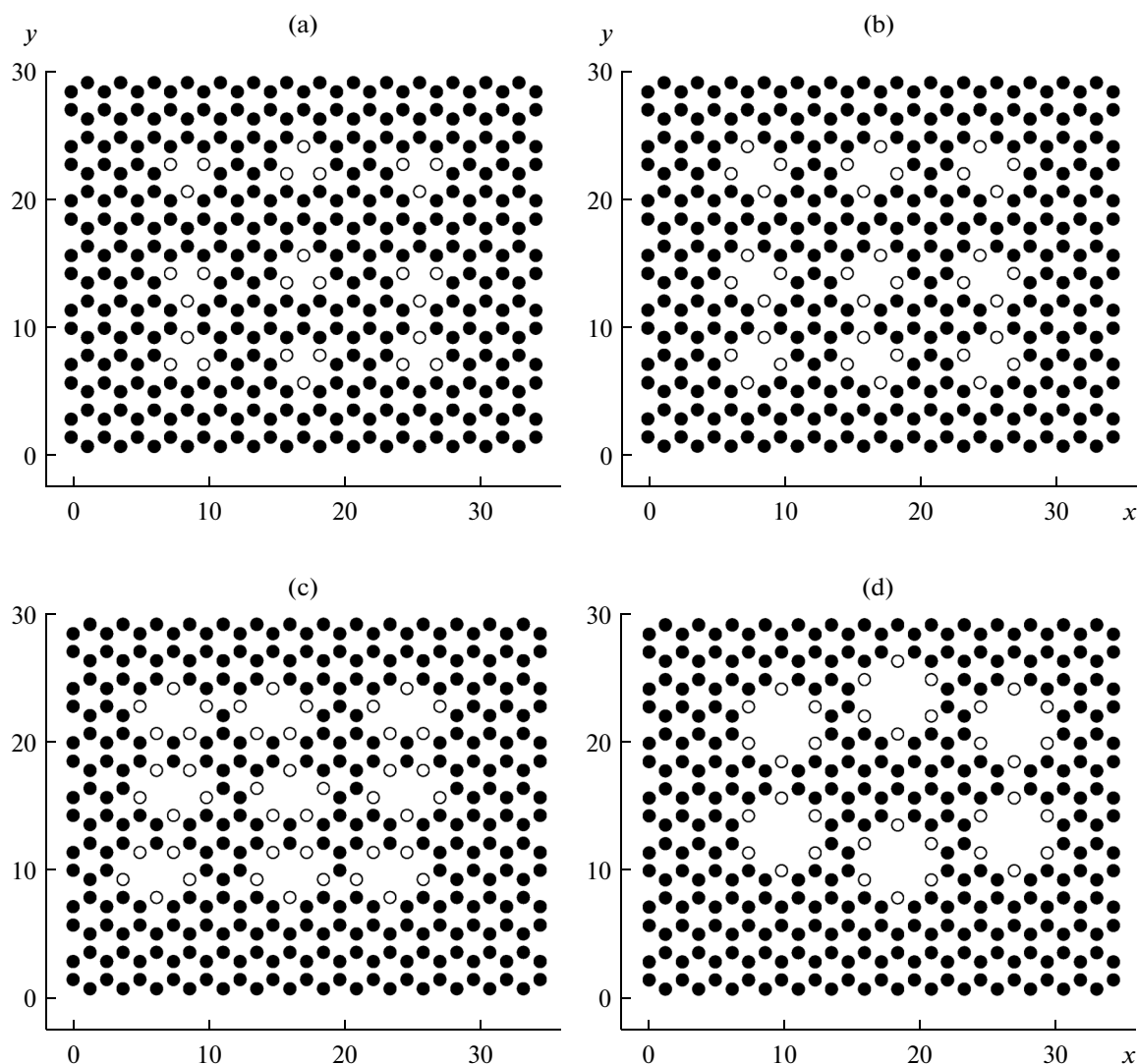


Fig. 1. Modified graphene sheets with (a) monovacancies, (b) bivacancies; (c) trivacancies, (d) hexavacancies, (solid circles) C atoms, (open circles) C atoms with added H atoms.

the best way for rectifying the trajectory of the Li⁺ ion in a flat channel under the effect of a constant electric field with intensity of 10^3 V/m. In the initial moment, by means of a random numbers generator, the lower part of the cell was filled with 10 Li⁺ ions each with the electric charge of $+1.0 e$, where e is the elemental electric charge. The directed motion of ions (upward) was provided by the positive electric charge of $+10 e$ at the lower base of the cell and the negative charge of $-10 e$ at its upper base. Each of these charges was created by 10 identical point charges. Such virtual capacitor acted on the model cell during the first 4 million time steps $\Delta t = 2 \times 10^{-16}$ s. To further randomize the ion transport in the cell, we used the effect of migrating electric charges (positive in the lower base of the cell and negative in its upper base). Charge migration along the bases of the model cell was achieved by means of a random numbers generator which changed

the position of charges in each time step. After the “Charging” period (4 million time steps), Li⁺ ions that reached the upper base lost their charge. Then, for the next 8 million time steps, we monitored the behavior of the system in the absence of electric charges at the ends of the cell and in the presence of a constant electric field with intensity of 10^3 V/m that transferred the still remaining Li⁺ ions in the opposite direction.

The transport of Li⁺ ions through pores in membranes was put under special control. The membrane could be crossed by an ion only in a point (on the membrane plane) within a circle of effective radius of one or another pore. The ion could find a pore by the presence of fractional electric charges on its perimeter. The charges were ascribed to both CH groups and the equal number of C atoms randomly chosen among the boundary atoms of each pore. The number of CH groups corresponded to the number of its nearest

neighbors (of C atoms) to the pore center. Thus, we had 3 such bonds for monovacancies, 4 for bivacancies, 5 for trivacancies, and 6 for hexavacancies. The CH group was described according to the monoatomic scheme [9]. This scheme was created when developing the migrating force fields used in predicting the thermodynamic properties of complex molecules [13]. The positive charges of CH groups and the negative charges of C atoms free of hydrogen at the pore edges were of the fluctuating nature preset by the random numbers generator. The maximum charge value for the CH group (+0.35 e) created a Coulomb potential for the Li⁺ ion motion which corresponded to the energy barrier to diffusion of a Li atom on the graphene sheet over the vertices of C atoms [14]. The calculations by the density functional method suggest the alternating-sign nature of fluctuations of the charge of atoms in the vicinity of graphene-sheet pores [15]. In our model, the fluctuating charge of CH groups and C atoms varied in the interval $-0.35 \leq q_{\text{CH}} \leq 0.35 e$.

The Tersoff potential used for describing the interatomic interactions in graphene is based on the bond order concept. The potential energy between two neighboring atoms i and j is described as [16]

$$V_{ij} = f_C(r_{ij}) \left[A \exp(-\lambda^{(1)} r_{ij}) - B b_{ij} \exp(-\lambda^{(2)} r_{ij}) \right], \quad (1)$$

$$f_C(r_{ij}) = \begin{cases} 1, & r_{ij} < R^{(1)}, \\ \frac{1}{2} + \frac{1}{2} \cos[\pi(r_{ij} - R^{(1)}) / (R^{(2)} - R^{(1)})], & R^{(1)} < r_{ij} < R^{(2)}, \\ 0, & r_{ij} > R^{(2)}, \end{cases} \quad (2)$$

where b_{ij} is the multiparticle parameter of the bond order which describes how the bond formation energy (the attractive part V_{ij}) is formed at the local accommodation of atoms due to the presence of the other neighboring atoms. The potential energy is the multiparticle function of positions of atoms i, j , and k and determined by parameters

$$b_{ij} = (1 + \beta \xi_{ij}^{n_i})^{-1/(2n)}, \quad (3)$$

$$\xi_{ij} = \sum_{k \neq i, j} f_C(r_{ik}) g(\theta_{ijk}), \quad (4)$$

$$g(\theta_{ijk}) = 1 + \frac{c^2}{d^2} - \frac{c^2}{\left[d^2 + (h - \cos \theta_{ijk})^2 \right]}, \quad (5)$$

where ξ is the effective coordination number, $g(\theta_{ijk})$ is the function of the angle between r_{ij} and r_{ik} which stabilizes the tetrahedral structure. For the most part, we took the parameters of the Tersoff potential for carbon from [16] but increased the distance of covalent bonding to 0.23 nm and included the additional weak attraction at $r > 0.23$ nm defined by the Lennard-Jones (LJ) potential with parameters taken from [17]. To eliminate the resulting angular momentum, in each graphene-

sheet site, the rotation component of the force created by atoms in the neighboring sites was eliminated. The analytical form of the local rotation potential of interaction was given in [17].

The Coulomb interaction was present between all electric charges in the system, i.e., Li⁺ ions, wandering point charges on cell ends, and fluctuating charges located in the pore vicinity. Furthermore, Li atoms and ions experienced the LJ interaction with the potential parameters taken from [18]. The LJ potential parameterized in [9, 19] was used in describing the interactions between CH groups and also in Li⁽⁺⁾-C pairs. The LJ interaction was also present between the following pairs of atoms: C-CH, Li⁽⁺⁾-CH. The parentheses in the superscript pointed to the possibility of charge disappearance. The parameters of the potential for these interactions were found in accordance with the Berthelot-Lorentz rule. Table 2 shows the parameters of all potentials used and the value and sign of charges present in the system.

The moderate removal of liberated heat from the system was accomplished according to the Berendsen scheme with the binding constant $\tau = 4$ fs [20]. To control the heating, in each time step, the velocities v were scaled as follows:

$$v = \lambda v, \quad \lambda = \left[1 + \frac{\Delta t}{\tau} \left(\frac{T_0}{T} - 1 \right) \right]^{1/2}, \quad (6)$$

where λ is the scaling factor, T_0 is the preset temperature (300 K), T is the current temperature.

The self-diffusion coefficient was calculated based on the mean square deviation of atomic movements $\langle [\Delta \mathbf{r}(t)]^2 \rangle$ [21]

$$D = D_{xy} + D_z = \lim_{t \rightarrow \infty} \frac{1}{2\Gamma t} \langle [\Delta \mathbf{r}(t)]^2 \rangle_n, \quad (7)$$

where $\Gamma = 3$ is the space dimension. The angle brackets $\langle \dots \rangle$ meant the averaging with respect to time, n is the number of time intervals for determination of $\langle [\Delta \mathbf{r}(t)]^2 \rangle$. Here, the time average was determined by averaging 20 curves each calculated in the interval of 40 ps (or 200000 Δt).

To calculate stresses, each graphene sheet was divided into unit areas. The atomic stresses $\sigma_J(l)$ in an unit area with the number l for each of directions x, y, z and with the running index J were determined by calculating kinetic energies of atoms in this area and the projections of forces f_J^i that acted on the l area from all other atoms [22]

$$\sigma_J(l) = \frac{1}{N} \left\langle \sum_i^k \frac{1}{\Omega} (m v_J^i v_J^i) \right\rangle + \frac{1}{S_l} \left\langle \sum_i^k (f_J^i) \right\rangle, \quad (8)$$

where N is the number of atoms in area l , Ω is the volume per atom, m is the atomic mass, v_J^i is the projection of the velocity of the i th atom, S_l is the surface of

Table 2. Parameters of Tersoff (for carbon) and Lennard-Jones potentials, the value and number of charges in the system

Parameters	Carbon	Interactions	σ , Å	ϵ , eV
A , eV	1.3936×10^3	C–C	3.400	0.00284
B , eV	3.4674×10^2	Li–Li	1.506	0.71597
$\lambda^{(1)}$, Å ⁻¹	3.4879	Li–C	2.473	0.00433
$\lambda^{(2)}$, Å ⁻¹	2.2119	Li–CH	2.638	0.05327
β	1.5724×10^{-7}	C–CH	3.535	0.04554
n	7.2751×10^{-1}	CH–CH	3.7700	0.00396
c	3.8049×10^4	Charges	Charge value, e	Number of charges
d	4.384	$q_{\text{Li}^+}(q_{\text{Li}})$	+1(0)	10
h	-0.57058	q_{lb}	+1	10
$R^{(1)}$, Å	1.8	q_{hb}	-1	10
$R^{(2)}$, Å	2.3	q_{CH}	0...0.35	54–90
–	–	q_{Cpore}	-0.35...0	54–90

l area. With this definition, the compressive stresses could have sign “+” or “-” depending on directions of forces f_j^i . This is the difference of a microscopic stress $\sigma_j(l)$ from a macroscopic stress $\bar{\sigma}_j < 0$.

In the problem to be solved, we are interested in the additional stresses in graphene sheets caused by migration of lithium ions through pores rather than in the absolute values of stresses in graphene determined by Eq. (8). In other words, the effect of ions on graphene was found based on the distribution of the differential characteristic $\Delta\sigma_j(l)$:

$$\Delta\sigma_j(l) = \sigma_j(l) - \sigma_j^{\text{free}}(l), \quad (9)$$

where $\sigma_j^{\text{free}}(l)$ represents the stress on the l area created by forces in the J direction in the absence of Li⁺ ions.

The calculations at $T = 300$ K in terms of the chosen model produced the total energy value for free single-sheet graphene equal to -7.02 eV, which agrees with the result of quantum mechanical calculations (-6.98 eV) [23]. It is known that an uncharged lithium atom is adsorbed in the vicinity of a vacancy on graphene, being bound to the surface by the energy even higher than that of lithium cohesion (0.36 eV/atom). Calculated in terms of the density functional theory, the binding energy of hydrogen atom with defective graphene is 0.875 eV/atom [24]. In a separate MD calculation, the binding energy of a Li atom with graphene containing bivacancies was assessed as ~ 0.4 eV/atom. The alternating-sign fluctuating charge near the pores in graphene allows the lithium ions to overcome the energy barrier and avoid retardation near the defects.

RESULTS OF CALCULATIONS

The best result of Li⁺ ion passage through membranes was achieved in version 4 (Fig. 2). In the latter case, 9 of 10 ions have reached the upper base of the cell after 4 million time steps and only one ion was hindered by the lower membrane to this moment. In the worst version 2, after 4 million time steps, 6 Li⁺ ions found themselves immediately at the upper base and one ion has just penetrated through a pore in the second (upper) membrane, 2 ions have passed the first membrane, and one ion was still in the lower chamber of the cell. To the end of the “Charging” process, in the other versions, 7 Li⁺ ions were present in the upper chamber and the largest number of ions (two) still stayed in the lower chamber of the membrane combination (version 1). The latter fact is explained by the difficulty for Li⁺ to pass through monovacancies.

The observed trajectories of Li⁺ ion migration represented broken lines with turning points on the walls of the basic cell or on graphene membranes. The similar trajectories were observed for migration of particles in dilute gases in presence of obstacles to their motion. Figure 3 shows typical trajectories of ions in the cell with the membrane set of version 4. Figure 3a reflects the travel of ions during the “Charging” process of the graphene–lithium device and Fig. 3b reproduces the trajectories of the resulting atoms after switching-on of a constant electric field with intensity of 10^3 V/m. Although the time interval corresponding to trajectories in Fig. 3a is twice shorter than the period corresponding to trajectories shown in Fig. 3b, the paths passed by ions in the former case considerably exceed the extent of their migration in the latter

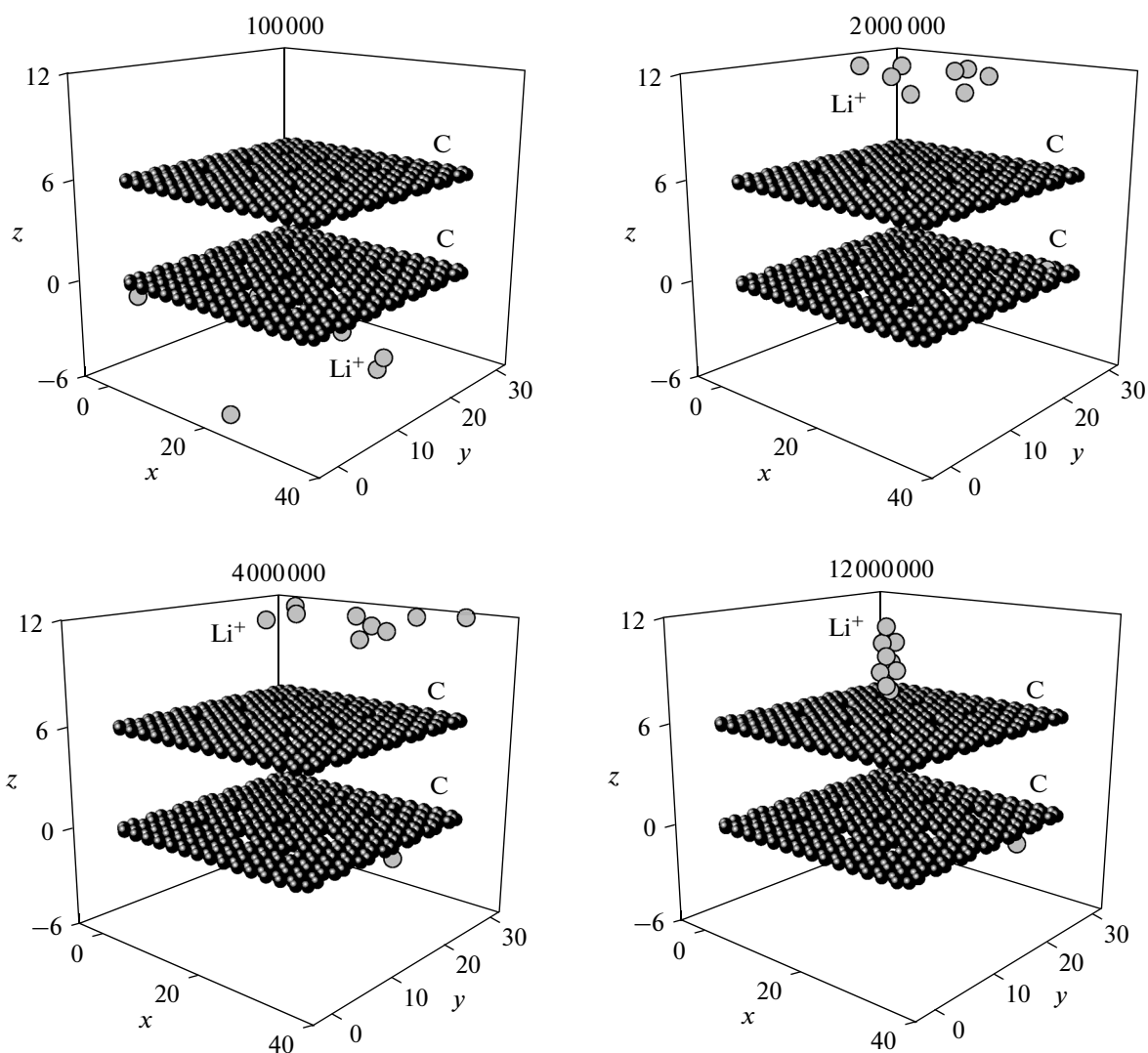


Fig. 2. Basic cell with membrane combination of version 4 in different moments. Numbers correspond to the number of time steps. Coordinates of atoms are shown in Angströms.

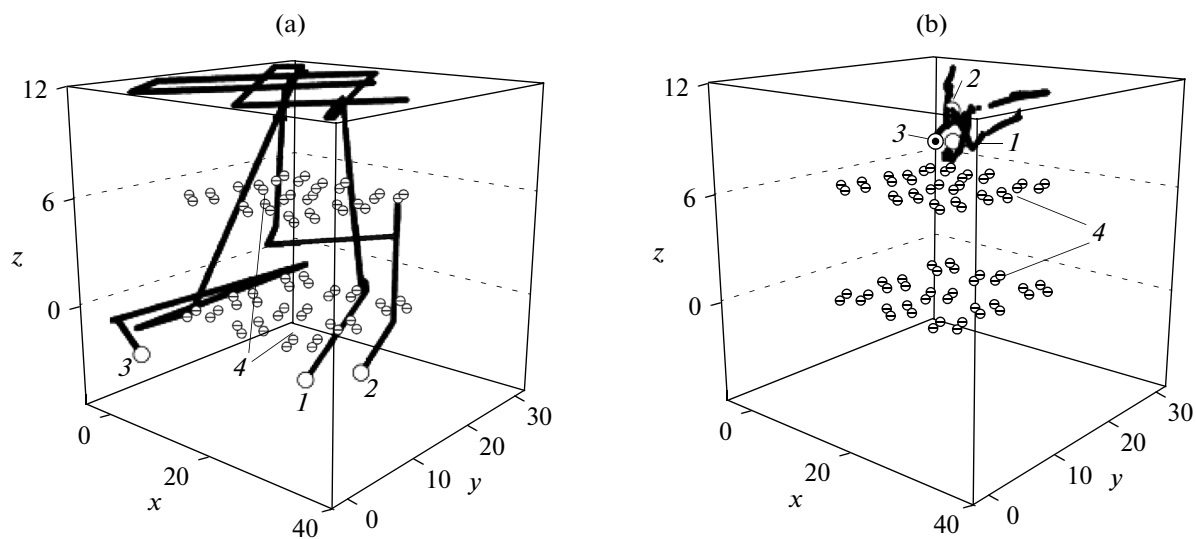


Fig. 3. Trajectories of three Li^+ ions during the following periods: (a) “Charging” (4 million time steps) and (b) “Discharge” (8 million time steps); numbers 1–3 indicate (a) initial and (b) final points of trajectories; (4) CH bond converged to a point.

case. In the concluding stage of “Charging”, Li⁺ ions wander near the upper base of the basic cell. At the constant electric field, Li atoms and ions have smoother trajectories localized in a rather limited space. In the other versions of membrane combinations, the trajectories of ions and atoms are much similar to those shown in Fig. 3.

The coefficients of mobility of Li⁺ ions in both horizontal (D_{xy}) and vertical (D_z) directions tend to decrease after the first 1 million time steps in the “Charging” process or $n = 5$ (Fig. 4). Note that interval values of D_{xy} and D_z change at a still higher rate. However, in the initial stage of “Charging” for different graphene membrane combinations, the coefficient D_{xy} can both increase and decrease (Fig. 4a). The coefficient D_z , in contrast, increases in this stage of “Charging” for all six versions. The steady decrease in D_z is observed only in version 2 and a weak short-term increase of this coefficient is observed for version 1 in the initial period of calculations. Obviously, the initial rise in coefficients D_{xy} and D_z is associated with the fact that the ions have acquired a certain energy level due to mutual repulsion and also with the increase in the migration volume due to their ability to penetrate through membranes. The subsequent steady decrease in these coefficients is explained by the gradual decrease in the volume accessible for migration, because ions approach the upper base of the cell and also by the low probability of their motion in the opposite direction. The highest values of D_{xy} and the smallest values of D_z are observed for the system with version 2 of membrane combination. Here, the highest mobility of Li⁺ ions in horizontal directions is combined with their lowest mobility in the vertical direction. The direct opposite to this case is version 4 where the minimum mobility of ions in horizontal directions is compensated by the highest mobility in the direction perpendicular to the membrane plane. The mutual compensation of values D_{xy} and D_z is observed also for the other versions of membrane combinations.

The ratio of throughput capacities of membrane combinations tested is confirmed also by the time dependence of the average level $z_{lev} = \frac{1}{n_{ion}} \sum_i^{n_{ion}} z_i$ (where z_i is the ion coordinate, n_{ion} is the number of ions) of elevation of Li⁺ in the system (Fig. 5). The highest average elevation of ions in the cell is observed for membranes in version 4 and the lowest elevation is observed for versions 6, 2, and 1. In all the cases, the point of the highest elevation of ions is reached in the immediate proximity of the end of “Charging”, i.e., after 4 millions time steps. Upon reaching the upper negatively charged plate of the external “capacitor”, the positively charged lithium ions should be electrically neutralized as a result of charge flow. This is why the contact with the upper wall of the basic cell is accompanied by the withdrawal of the charge from the

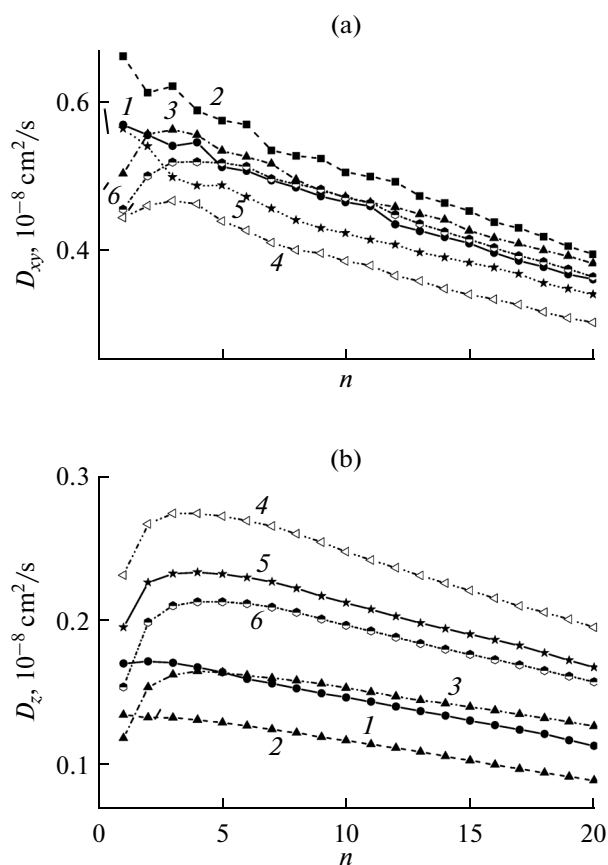


Fig. 4. (a) Horizontal and (b) vertical components of the mobility coefficient of Li⁺ atoms; numbers correspond to the versions of membrane combinations shown in Fig. 1.

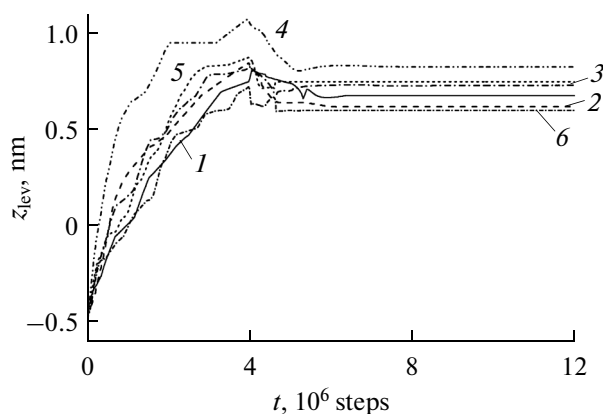


Fig. 5. The average elevation level of Li⁺ ions in the basic cell; numbers correspond to versions of graphene membrane combinations.

ion. The end of “Charging” in this model means the end of operation of the virtual external “capacitor”. The “Charging” process proves to be feasible in the presence of the external “capacitor” and infeasible when a constant electric field with intensity of 10^3 and

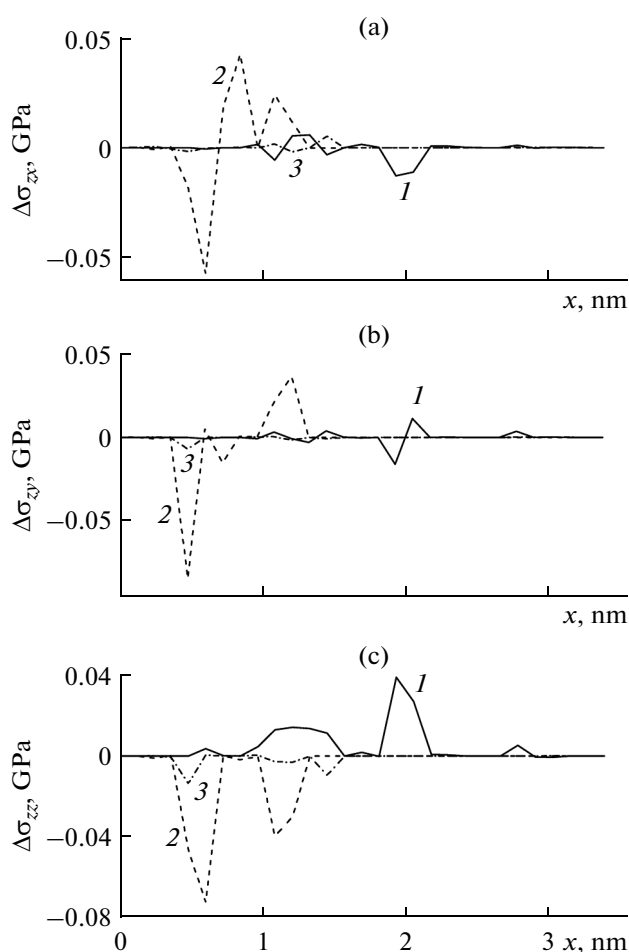


Fig. 6. “Charging”-period-averaged stresses generated in the plane of graphene membranes during the passage of Li^+ ions.

10^4 V/m is applied. Instead of moving up through membranes, the ions stay in the lower chamber near the walls. The “Discharge” process starts with switching-on of a constant electric field with intensity $E = 10^3$ V/m to induce the opposite motion of ions. It deserves mention that the ions, after reaching the upper base of the cell and losing their electric charge to acquire the status of atoms, inherit together with this status the trend towards cluster formation. In all cases without exception, after 12 million time steps, Li atoms in the upper chamber aggregated into clusters, which prevented them from returning down through the upper membrane (Fig. 3b). Moreover, the clusters formed always were in contact with graphene. Switching-on of a constant electric field to induce the opposite travel of ions gives rise to a sufficiently fast (within 1.8 million time steps) but weak decrease in the value z_{lev} . In 2 million steps from the beginning of “Discharge”, the dependence $z_{\text{lev}}(t)$ represents horizontal segments in

all the cases. This is associated with the formation of clusters of Li atoms in the upper chamber of the cell and adhesion of Li^+ ions to the graphene surface.

The effect exerted on graphene by migrating Li^+ ions was assessed based on the spatial distribution of differential components of the stress tensor $\Delta\sigma_J(l)$. The division of graphene sheets into strips prolate along the “chair” direction makes it possible to calculate the distribution of stress tensor components along the “zigzag” direction. Figure 6 shows the calculated distributions for components $\Delta\sigma_{zx}$, $\Delta\sigma_{zy}$, and $\Delta\sigma_{zz}$. Curves 1, 2, and 3 pertain to systems with membrane combinations of versions 1, 2, and 4. The sign of these local stresses is determined by the direction of forces acting on the corresponding unit areas and carries no information on the nature of produced deformation, unlike the case of macrostresses. The character of the effect of Li^+ ions on Li^+ -permeable membranes of modified graphene is clearly manifested in the distribution of stresses produced during “Charging”. On the whole, a clear relationship can be traced between the stresses created in membrane planes and the throughput of membranes with respect to ions: the easier the ions penetrate the membranes, i.e., the higher the permeability of modified graphene, the lower the stresses left by ions after their penetration. Here, the pore size does not play any decisive role. Thus, version 2 of membrane combination has in total the larger pores as compared with version 1. However, due to elimination of the possibility of straight-through penetration of both membranes (due to their shift) by a rectilinearly moving ion, the stresses created in membranes of version 2 are higher as compared with version 1. Furthermore, this concerns the stress tensor components created by both horizontal and vertical forces. Note also that for version 1, the significant stresses are distributed over the larger surface of membranes as compared with version 2. Among the simulated basic cells, the lowest stresses in membranes created by passing ions are observed for version 4. In the latter case, the stress $\Delta\sigma_{zz}$ associated with the action of vertical forces is much higher than the stresses $\Delta\sigma_{zx}$ and $\Delta\sigma_{zy}$ caused by horizontal forces. For this version, the purely local nature of stress distribution in membranes is manifested.

DISCUSSION

The above calculations demonstrated that for the lowest characteristics of membrane crossing (versions 1, 2, and 6), the scatter in the velocities of Li^+ ions when they pass the partitions may reach 73%, whereas for the best crossing characteristics (version 4), the scatter does not exceed 25%. Studying the angle θ at which the trajectories of migrating ions intersect the membranes has shown that the angle θ averaged over the

number of ions does not differ too much between the successful and failed versions of penetration through membranes. Thus, for version 4, this angle is 56.2°, whereas for version 1, 2, and 6, the θ angle is equal to 55.2°, 63.4°, and 53.1°, respectively. At the same time, the difference in the dispersion of angle θ distribution over ions turned out to be very significant for the cases of good and bad penetration through membranes. For version 4, the dispersion of his angle is 4.5°, whereas for versions 1, 2, and 6 the dispersion is 29.8°, 14.9°, and 14.3°, respectively.

Version 4, the most efficient as regards penetration of Li⁺ ions corresponds to two graphene sheets each containing 9 bivacancies. Apparently, the high permeability of this version is explained by the fact that it has the optimal combination of geometrical and electrical properties of pores. The ratio n_H/n_{VC} , where n_H is the number of hydrogen atoms pertaining to one pore and n_{VC} is the number of C atoms removed during the pore formation can serve as a criterion of the efficient permeability of pores. The ratio n_H/n_{VC} is 3.0, 2.0, 1.67, and 1.0 for mono-, bi-, tri-, and hexavacancies, respectively. The high ratio n_H/n_{VC} of monovacancies fails to provide efficient migration, because it is difficult for ions to pass through very small pores. However, already in the second position of this series (=2), n_H/n_{VC} correctly reflects the degree of efficient penetration through membranes.

Understanding the role of lattice defects and functional groups on a graphene membrane is very important for operation of the Li–air battery. Because Li₂O₂ has predominant growth points and the size of resulting particles is limited by defects, the possibility appears of tuning the energy/power ratio for certain energy applications by controlling the defects and functional groups on the graphene surface. Such structural control may be very useful for rechargeable Li–air cells. It was shown [4] that in the vicinity of defects, the coarsening of Li₂O₂ clusters is disadvantageous as regards energy. This is why, at the deposition of Li₂O₂, isolated nanosized islets are formed, which ensures smooth transport of oxygen during the discharge process. Limiting the size of reaction products makes it possible to improve the rechargeability of Li–air batteries because prevents the gradual increase in the total resistance of the electrode and provides the better access to the catalyst during the charging process.

CONCLUSIONS

The migration of lithium ions through graphene membranes containing different kinds of pores was studied. The migration of Li⁺ ions occurred under the effect of fluctuating electric charges of the corresponding sign which were present at end faces of the basic cell in the “Charging” period of the modeled electrode. Each of two graphene sheets used had 9 or 6 pores of certain type. The pores represented monovacancies,

bivacancies, trivacancies, and hexavacancies. The graphene sheets were partly hydrogenated. Atoms H were added to the edge C atoms the closest to the pore center. The CH group was described in terms of a combined atomic scheme and had a positive fluctuating electric charge. The gap between graphene membranes was sufficient for migration of Li⁺ ions under the effect of a constant electric field. Among six membrane pairs under study, the most efficient was the pair of two identical graphene sheets containing bivacancies. Moreover, the close-to-equilibrium distribution of bivacancies in each sheet was shifted by ~ 0.2 nm in order to prevent ions from the straight-through crossing of two membranes at once. The loss of electric charge by Li⁺ ions resulted in the formation of a lithium cluster insensitive to the electrostatic directing force. Moreover, in a constant electric field, Li⁺ ions “adhered” to membranes due to their high adhesion to graphene. These factors complicated the “Discharge” process in the device under consideration. The ions developed very short back trajectories. In the “Discharge” period, for the efficiently permeable membrane pair, Li⁺ ions exhibited the lowest mobility in horizontal directions and the highest mobility in the vertical direction. For inefficiently working membrane pairs, the inverse situation was true. The average level of vertical travels of ions in the system can be also used in assessing the efficiency of membrane pairs. The time dependence of the latter level makes it possible to determine the extent and duration of the “charging” stage. The Li⁺ ions passing through membranes generate predominantly local stresses in graphene sheets. The developed stresses decreased with the increase in membrane permeability. As a rule, the stresses generated by vertically oriented forces were comparable with those created by horizontally oriented forces.

REFERENCES

1. Novoselov, K.S., Geim, A.K., Morozov, S.V., Jiang, D., Katsnelson, M.I., Grigorieva, I.V., Dubonos, S.V., and Firsov, A.A., *Nature*, 2005, vol. 438, p. 197.
2. Segal, M., *Nat. Nanotechnol.*, 2009, vol. 4, p. 611.
3. Zhu, Y.W., Murali, S., Stoller, M.D., Ganesh, K.J., Cai, W.W., Ferreira, P.J., Pirkle, A., Wallace, R.M., Cychosz, K.A., Thommes, M., Su, D., Stach, E.A., and Ruoff, R.S., *Science*, 2011, vol. 332, p. 1537.
4. Xiao, J., Mei, D., Li, X., Xu, W., Wang, D., Graff, G.L., Bennett, W.D., Nie, Z., Saraf, L.V., Aksay, I.A., Liu, J., and Zhang, J.-G., *Nano Lett.*, 2011, vol. 11, p. 5071.
5. Huard, B., Sulpizio, J.A., Stander, N., Todd, K., Yang, B., and Goldhaber-Gordon, D., *Phys. Rev. Lett.*, 2009, vol. 102, p. 026807.
6. Krekora, P., Su, Q., and Grobe, R., *Phys. Rev. Lett.*, 2004, vol. 92, p. 040406.
7. Setare, M.R. and Jahani, D., *Phys. B*, 2010, vol. 405, p. 1433.
8. Allain, P.E. and Fuchs, J.N., *Eur. Phys. J. B*, 2011, vol. 83, p. 301.

9. Lamari, F.D. and Levesque, D., *Carbon*, 2011, vol. 49, p. 5196.
10. Pei, Q.X., Zhang, Y.W., and Shenoy, V.B., *Carbon*, 2010, vol. 48, p. 898.
11. Rangel, E., Vazquez, G., Magana, F., and Sansores, E., *J. Mol. Model.*, 2012, vol. 18, p. 5029.
12. Gautam, S., Dharamvir, K., and Goel, N., *J. Phys. Chem. A*, 2011, vol. 115, p. 6383.
13. Wick, C.D., Martin, M.G., and Siepmann, J.I., *J. Chem. Phys. B*, 2000, vol. 104, p. 8008.
14. Ataca, C., Akturk, E., Ciraci, S., and Ustunel, H., *Appl. Phys. Lett.*, 2008, vol. 93, p. 043123.
15. Kheirabadi, N. and Shafiekhani, A., *Phys. E (Amsterdam, Neth.)*, 2013, vol. 47, p. 309.
16. Tersoff, J., *Phys. Rev. Lett.*, 1988, vol. 61, p. 2879.
17. Stuart, S.J., Tutein, A.V., and Harrison, J.A., *J. Chem. Phys.*, 2000, vol. 112, p. 6472.
18. Tao, Z. and Cummings, P.T., *Mol. Simul.*, 2007, vol. 33, p. 1255.
19. Chan, Y. and Hill, J.M., *Micro Nano Lett.*, 2010, vol. 5, p. 247.
20. Berendsen, H.J.C., Postma, J.P.M., van Gunsteren, W.F., DiNola, A., and Haak, J.R., *J. Chem. Phys.*, 1984, vol. 81, p. 3684.
21. Galashev, A.Y. and Polukhin, V.A., *J. Surf. Invest.: X-ray, Synchrotron Neutron Tech.*, 2014, vol. 8, p. 1078.
22. Galashev, A.E., *Tech. Phys.*, 2014 vol. 59, no. 4, p. 467.
23. Davydov, S.Yu., *Phys. Solid State*, 2012, vol. 54. no. 4, p. 875.
24. Rangel, E., Ramirez-Arellano, J.M., Carrillo, I., and Magana, L.F., *Int. J. Hydrogen Energy*, 2011, vol. 36, p. 3657.

Translated by T. Safonova